Available online at www.sciencedirect.com
SCIENCE DIRECT®
Biochimica et Biophysica Acta 1615 (2003) 93–102
BIOCHIMICA ET BIOPHYSICA ACTA
BBA
www.bba-direct.com

Humicola lanuginosa lipase hydrolysis of mono-oleoyl-rac-glycerol at the lipid–water interface observed by atomic force microscopy

Konstantin Balashev[a], Martin Gudmand[a], Lars Iversen[a], Thomas H. Callisen[b], Allan Svendsen[b], Thomas Bjørnholm[a,*]

[a] *Department of Chemistry, Nano-Science Center, University of Copenhagen, Universitetsparken 5, 2100 Copenhagen, Denmark*
[b] *Novozymes, Smørmosevej 25, DK-2880 Bagsværd, Denmark*

Received 6 February 2003; received in revised form 13 June 2003; accepted 4 July 2003

Abstract

A new type of planar lipid substrate for *Humicola lanuginosa* lipase (HLL) has been prepared by depositing a monolayer of 1-mono-oleoyl-rac-glycerol (MOG) on top of a monolayer of dipalmitoyl-phosphatidylcholine (DPPC) on mica by the Langmuir–Blodgett (LB) technique. The bilayer was subsequently exposed to HLL in a liquid cell of an atomic force microscope (AFM) allowing the time course of the lipolytic degradation to be observed. By analysing a series of AFM images, we find that enzymes are preferentially activated at the edge of nano-scale defects present in the bilayer prior to enzyme injection, while defect-free areas of the substrate are surprisingly stable towards enzyme degradation. The initial rate of hydrolysis is found to be proportional to the perimeter length, P, of the initial nano-scale defects as well as the bulk enzyme concentration, c_{HLL}; $d(\text{lipid})/dt = k\,P\,c_{HLL}$. We estimate the specific rate of MOG hydrolysis by HLL to be 2.5×10^4 MOG molecules/(minute·molecule of HLL).

Keywords: Atomic force microscopy; *Humicola lanuginosa* lipase; Supported bilayer; Interfacial enzyme kinetics

1. Introduction

The atomic force microscope (AFM), invented in 1986 by Binnig et al. [1], is rapidly growing as a method for studying the nano-scale structure of a wide range of materials spanning from inorganic semiconductors to biochemical systems [2]. Initially, it was demonstrated by Prater et al. [3] that AFM could also be applied to operate in buffer solutions. This paved the way for studies of enzyme structure and enzyme behaviour in organized molecular media which mimics in vivo systems, as recently reviewed [2,4]. Direct observation of single enzyme activity, demonstrated by Radmacher et al. [5], was the first step which revealed the potential of AFM as an instrument for studying dynamics and evolution of enzymatic processes. The direct visual evidence of supported bilayer hydrolysis by phospholipase A_2 (PLA_2) was later presented by Grandbois et al. [6], and recently Nielsen et al. [7,8] have used AFM to visualize lag-burst kinetics of PLA_2 and related it to the nano-scale heterogeneity of the substrate bilayers.

Lipases (triglyceride hydrolases) are a group of structurally well-characterised interfacially activated enzymes [9,10], which have virtually zero activity on monomeric substrate molecules and high activity on organized substrate molecules constituting a lipid–water interface [11]. *Humicola lanuginosa* lipase (HLL) is part of a subfamily of lipases from microorganisms that all have the same active site defined by a Ser–His–Asp triad [12]. The active site in HLL is accessible only through a hydrophobic pocket which is covered by a "lid", constituted by a two-turn α-helix which can roll-over, giving rise to at least two different conformations, an inactive form with the lid closed and an active form with the lid open [9,13]. The open form with the lid rolled over is favoured in media of low dielectric strength, e.g. the lipid–water interface [14–16].

Triglyceride lipases have always received considerable attention as they have diverse physiological function in food and fats degradation [17]; however, the study of the

* Corresponding author. Tel.: +45-3532-1835/00; fax: +45-3532-0460.
E-mail address: tb@nano.ku.dk (T. Bjørnholm).

0005-2736/$ - see front matter © 2003 Elsevier B.V. All rights reserved.
doi:10.1016/S0005-2736(03)00209-8

enzyme reaction kinetics in organized substrate media still faces difficulties due to the very weak amphiphilic nature of the triglyceride substrate molecules. They are virtually insoluble in water and either absorbs on the available surfaces or forms droplets of uncontrolled dispersity [13]. The problem with preparing organized and well-defined lipid substrates with known surface areas has made it extremely difficult to obtain kinetic constants for lipase reactions. So far, only one complete set of kinetics constant for HLL hydrolysis has been determined using *p*-nitrophenylbutarate (PNPB) as substrate as guest in anionic 1-palmitoyl-2-oleoylglycero-*sn*-3-phosphoglycerol (POPG) vesicles [13]. Indirect evidence that HLL activation is induced by a curved anionic interface has also been presented by the same authors [13].

Recently hydrolysis of MOG by HLL has been performed using the ''zero-order trough'' technique [18]. Techniques for measuring interfacial lipolytic catalysis on monolayers were established by Verger and Haas [19] and developed systematically by two groups; Verger et al. [20,21] and Brockman et al. [22,23]. The monolayer technique has proven to be one of the most reliable methods for lipase kinetics studies. It has the advantage of control over the interfacial quality of the surface: molecular orientation, conformational state, packing density, molecular dipole moment and lateral viscosity can all be controlled by means of surface pressure and monolayer composition. Nevertheless, use of the monolayer technique for studying enzyme reactions at the air–water interface has limitations. It is not possible to study the detailed nanoscale structure of the monolayer (i.e. heterogeneity) and the monolayer is under constant lateral pressure, which keeps it densely packed during hydrolysis. In addition, it has, in the HLL case, proved necessary to add β-cyclodextrin to the water phase to solubilize the long chain fatty acid hydrolysis products [24].

In this study, we combine the advantages of the Langmuir–Blodgett (LB) technique and AFM technique to both visualize and analyse the degradation process of a supported bilayer immersed in water. We show how the AFM can be used as a tool for studying the kinetics of lipolytic degradation of a supported DPPC/MOG bilayer. This approach reveals crucial information regarding the mechanism of the lipolytic event at the molecular level and an estimate of the specific activity of HLL.

2. Materials and methods

2.1. Lipids

1,2-Dipalmitoyl-*sn*-glycero-3-phosphocholine (DPPC) and 1-mono-oleoyl-rac-glycerol (MOG) were purchased from Avanti Polar Lipids (Alabaster, AL) and Sigma (St. Louis, MO), respectively. Both lipid samples were used as received.

2.2. Enzyme

HLL was provided by Novozymes A/S and diluted with water (Milli-Q, pH ~ 6.5) to concentrations 2.5, 15 and 45 nM.

2.2.1. Bilayer preparation

The supported DPPC/MOG bilayers were prepared using the LB-technique on a commercial Langmuir through (KSV 5000, KSV Ltd., Finland). Freshly cleaved mica was used as solid support. DPPC was dissolved in HPLC grade *n*-hexane to a concentration of 0.6 mg/ml. MOG was dissolved in chloroform to a concentration of 1 mg/ml. All LB-experiments were done at room temperature, 20 °C. Initially, DPPC was spread on a pure Milli-Q water surface. Solvent evaporation was allowed for 30 min. Monolayer compression was done at constant velocity of 1 $Å^2$/molecule/min to a final surface pressure of 35 mN/m, corresponding to a mean molecular area (MMA) of 50 $Å^2$ [8,25], and transferred vertically at a constant speed of 1 mm/min. After cleaning the LB trough, MOG was spread on a pure Milli-Q water surface. Solvent evaporation was allowed for 10 min and compressed to a target pressure of 25 mN/m, corresponding to a MMA of 40 $Å^2$ [25,26]. The MOG monolayer was then transferred on top of the DPPC layer at a constant speed of 1 mm/min by vertical dipping. The final bilayer samples were kept immersed in water at all times prior to imaging.

2.2.2. AFM imaging

The supported bilayers were transferred to the liquid cell of the AFM (Nanoscope IIIa, Digital Instruments, Santa Barbara, CA) using a standard silicon O-ring to seal the liquid cell. Pure Milli-Q water was used to flush the liquid cell prior to imaging. Scanning was carried out using oxide sharpened silicon-nitride tips (NanoProbes, Santa Barbara, CA) with a nominal spring constant of 0.06 N/m. The bilayer and liquid cell was allowed to thermally equilibrate for at least 30 min before flushing the respective enzyme solution into the cell. Imaging was carried out in contact mode with a loading force of less than 500 pN at room temperature (25 °C). All experiments were repeated 2–3 times.

2.3. Analysis of the images

Image analysis was carried out using the public domain programs Image SXM on a Macintosh computer, and the PC equivalent programme Scion Image (both available on the internet at http://rsb.info.nih.gov/nih-image). Since the AFM scans took 1.5 min to complete, it was necessary to divide the AFM images into ''time zones''. Therefore, each structural defect was assigned an individual point of time (e.g. a defect in the top of a scan could be assigned $t = 1.7$ min, while another defect in the bottom of the same scan could be assigned $t = 2.8$ min). Furthermore, the aggregates observed inside some of the structural defects were ignored.

These aggregates do not directly influence the calculations of the rate of hydrolysis given that we measure the difference in the total area inside the edge of the holes.

3. Results and discussion

As mentioned, a substantial obstacle in lipase kinetics studies has been the preparation of well-defined substrates because simple lipids have a very weak amphiphilic nature. This has been overcome here by using a strongly amphiphilic phospholipid as a supporting first layer transferred to mica using the LB-technique. The DPPC-modified surface exhibits strongly hydrophobic qualities upon which a monolayer of MOG can be transferred, resulting in a well-defined planar MOG surface in which the headgroup of the lipid is exposed towards the aqueous solution containing enzyme. The prepared bilayers were all imaged using an AFM liquid cell. In a control experiment, one of the MOG/DPPC bilayers were imaged in the liquid cell AFM for 2 h prior to experiments to check for stability and tip–sample interaction effects. The bilayer was found to be stable during this period. After thermal equilibration of the liquid cell for a minimum of 30 min, the enzyme was injected into the cell and the change of lipid bilayer desorption was followed over time. We present in the following three typical performed experiments using three different concentrations of enzyme, 2.5, 15 and 45 nM. By varying the enzyme concentration prior to injection into the liquid cell and analysing the resulting sequence of real-time AFM images of changes in desorbed area of the DPPC/MOG bilayer, we measured the overall rate of desorption of lipid due to lipase action, i.e. the growth of holes as a function of time after injection of enzyme.

All prepared bilayers had initial structural defects (e.g. Fig. 1A). The height differences between the DPPC/MOG film (bright domains) and the mica (dark domains) in the 15 and 45 nM experiments were 3.5 ± 0.5 nm (see inset Fig. 1A). This value is in good agreement with the X-ray data for the thickness of a MOG monolayer which is approximately 1.3 nm [27] and the thickness of the DPPC monolayer which is approximately 2.4 nm [25]. The height difference between the DPPC/MOG film and the mica in the 2.5 nM experiments was 2.5 ± 0.5 nm. This lower value indicates that the lipid film relaxed after transfer, prior to imaging, and the surface density of the imaged film is expected to be slightly below the surface density of the MOG film in the LB-trough kept at a surface pressure of 25 mN/m.

The average area of a single structural defect in the three experiments using 2.5, 15, and 45 nM concentrations of the enzyme was 0.40, 1.01 and 0.42 μm^2, respectively.

In Fig. 1, a series of images from the 15 nM experiment is shown. The first image (Fig. 1A) is prior to enzyme injection. Images B–H show consecutive changes due to enzyme action, with a clear increase of desorbed area observed just a few minutes (~ 2 min) after enzyme injection into the liquid cell (Fig. 1B).

PLA_2 has been reported to preferably hydrolyse areas in the bilayer where product incubation has ripened the membrane [7,8]. For HLL, we observe that the edge of the holes is the most susceptible site for the enzyme attack. This is probably due to both the high curvature and loose molecular organization at the edge of the bilayer defect giving ideal conditions for enzyme penetration and activation.

In a quantitative analysis, all holes in the AFM images from all three concentrations of HLL (2.5, 15 and 45 nM) spanning the first 30 min were analysed with respect to the change in desorbed area (ΔA), the initial perimeter length (P_o), and the change in time (Δt). In the following, we refer to $\Delta A/\Delta t$ as the rate of hydrolysis and $\Delta A/\Delta t_o \cdot P_o$ as the normalised initial rate.

A plot of the desorbed area from each image series versus time (Fig. 2A) shows that almost equal amounts of lipid is desorbed in the first minutes of the 15 and 45 nM experiments, i.e. the initial rates of hydrolysis are nearly identical. They are not, as expected from Michaelis–Menten kinetics, proportional to the enzyme concentration [28]. This inconsistency can be explained by assuming that the perimeter length of the individual structural defects enter the rate equation as a measure of the effective substrate concentration. This hypothesis is supported by the qualitative analysis of the degradation mode which clearly shows how the edge of the structural defects constitutes the most potent enzyme activation sites. The relatively large initial defect in the 15 nM series, compared to the 45 nM series, hence accounts for the relatively large initial rates in the 15 nM series. Therefore, we propose that the initial rate obeys the relation;

$$v_{init} = k \cdot c_{HLL} \cdot P_o \quad (1)$$

where v_{init} is the initial rate ($\Delta A_o/\Delta t_o$), k is an empirical constant, c_{HLL} is the bulk concentration of enzyme and P_o is the initial perimeter length of the structural defects. To check the validity of Eq. (1), the initial change in desorbed area (ΔA_o) per initial perimeter length (P_o) plotted versus time (Δt) is shown in Fig. 2B. In this plot, the expected proportionality between initial rate per perimeter and enzyme concentration is observed as discussed further below. The plots (Fig. 2A and B) furthermore shows two well distinguishable phases in the rate of hydrolyses; an initial burst followed by a practically zero rate. Consequently, none of the bilayers are completely desorbed after 3 h of enzyme action. Actually, in all three experiments, the rate of hydrolysis is decreased dramatically after less than 30 min after enzyme injection. This incomplete hydrolysis suggests that the hydrolysis products, the desorbed DPPC or possibly both inhibit the enzyme. Most likely, the inhibition is caused by the extremely low CMC of DPPC (5×10^{-10} M) [29], which causes all desorbed DPPC molecules to form aggregates of admicelles, vesicles, etc. In the 2.5 nM experiment,

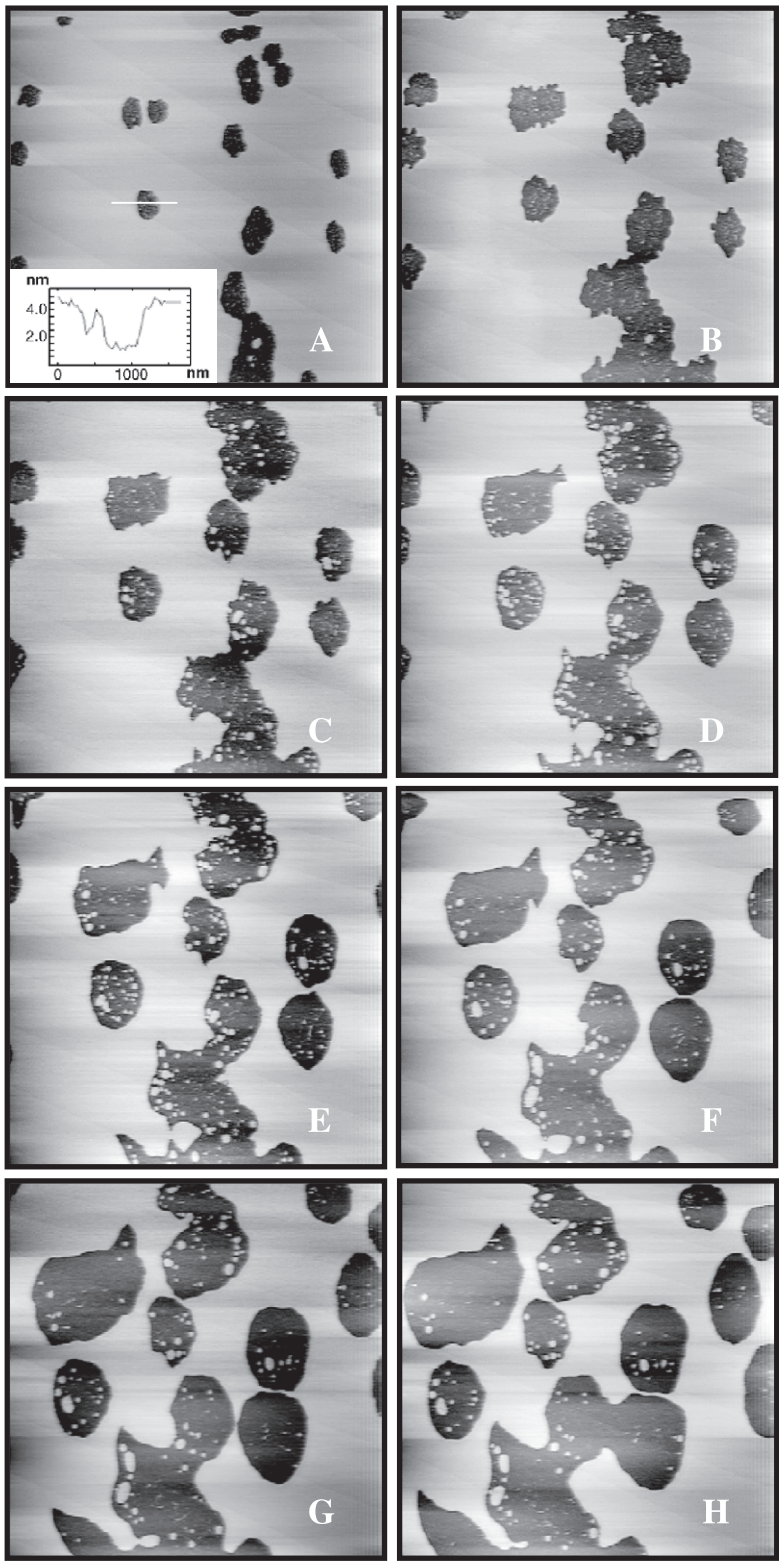

Fig. 1. Time sequence of AFM images from experiment where a 15 nM HLL solution was injected into the liquid cell (scan size 15×15 μm^2). Image (A) is prior to enzyme injection, (B) is 2–3 min after, (C–H) is selected images 5–180 min after enzyme injection. The dark areas are structural defects in the lipid bilayer. After enzyme injection, the initial structural defects expand as the top layer MOG is hydrolysed and the supporting DPPC layer spontaneously desorb. Inset (A) shows the height analysis (white line) of the double layer which is 3.5 nm deep.

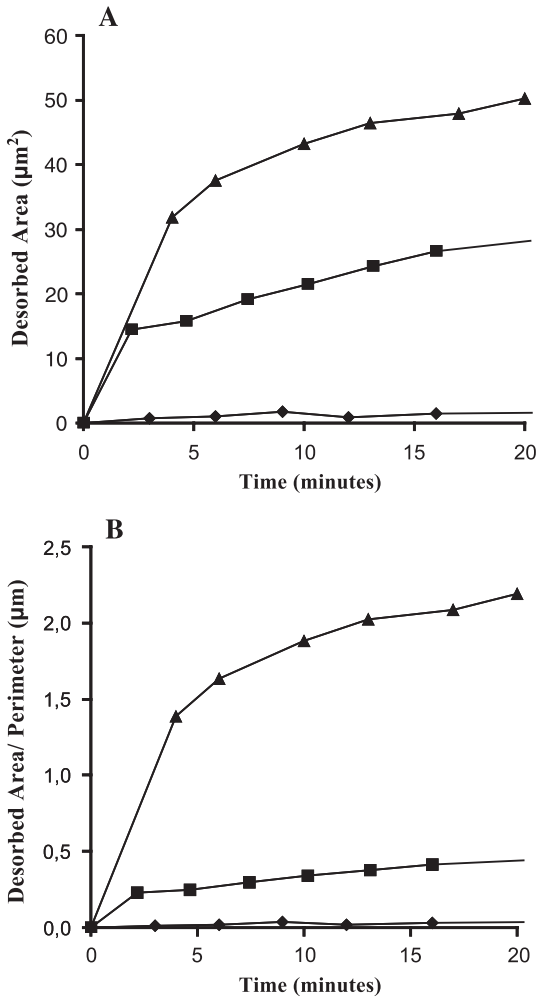

Fig. 2. Desorbed lipid area versus time after enzyme injection. (A) Curves for the three performed experiments using 2.5 nM (♦), 15 nM (■) and 45 nM (▲) concentration of enzyme, respectively. All three curves show the same characteristics where an initial burst in hydrolysis is followed by a lower (virtually zero) steady rate. The initial rate (=slope) of the 15 and 45 nM experiments is nearly superimposable and not as expected proportional to enzyme concentration. (B) The normalised initial rates (see text).

the desorbed area of DPPC in the first scan, approximately 3 min after enzyme injection, is 0.71 μm^2. The number of DPPC molecules corresponding to this area is 1.3×10^6 (desorbed area/MMA$_{DPPC}$). The same calculation for the two other experiments, 15 and 45 nM, yield the number of desorbed DPPC molecules after the first scan to be 2.9×10^7 and 6.4×10^7, respectively. Introducing the term scan area volume as the volume of water over the scan area, the concentration of DPPC can be estimated. Using a scan area volume of 5×10^{-11} dm^3 (scan area, 1×10^2 μm^2; height of liquid cell, 0.5 mm) the formal concentration of DPPC after 3 min is 5×10^{-8} M in the 2.5 nM experiment, 1×10^{-6} M in the 15 nM experiment and 2×10^{-6} M in the 45 nM experiment. In all cases, the CMC is exceeded several hundred times. The aggregates formed as a consequence of exceeding the CMC are ideal for binding free enzyme [14,30], and hydrolysis is most likely halted as a result of HLL binding to the DPPC aggregates. Another explanation of the incomplete hydrolysis is based on the formation of free fatty acids. Some of the fatty acids produced by hydrolysis of MOG may stay in the lipid layer. It has earlier been shown that formation of more than 5–10% free fatty acids in monolayers inhibit HLL's activity in monolayers [31]. Possible changes in the dielectric constant (ε) of the exposed monolayer surroundings could cause a decrease in number of functional enzymes on the lipid surface [16].

The mechanism for adsorption and activation of HLL at the lipid–water interfaces on vesicles has previously been proposed [21,32]. In our experiment, we observe that hydrolysis takes place at the edge of structural defects, and therefore these structural defects that are present before enzyme injection, expand after being exposed to HLL. At the same time, large areas that are void of structural defects are surprisingly stable during the duration of the experiment. We propose that this directly observed phenomena in the AFM experiment (Fig. 1) can be described by the following molecular events summarised in Fig. 3: the enzymes adsorb evenly to the lipid film [27] and they are preferentially activated at the edge of a structural defect (Fig. 3B). In a hypothesised rate-limiting step, HLL hydrolyses MOG to glycerol and oleic acid (Fig. 3C). The hydrolysis of MOG molecules leads to the exposure of DPPC's hydrophobic tail to the aqueous phase. In a kinetically fast step, these unfavourable oriented DPPC molecules spontaneously desorb and most likely form lipid aggregates (vesicles, admicelles, etc.), which are either dissolved in the aqueous phase (Fig. 3C) or remain as adsorbed aggregates inside the structural defects. In rare cases, we have observed this desorption step directly by AFM (data not shown). In the end, the hydrolysis of the lipid substrate is inhibited due to binding of all free enzymes to the formed DPPC aggregates of either soluble vesicles (Fig. 3D) or double layer structures formed at the solid–liquid interface (Fig. 3E). Alternatively, free fatty acids which remain at the interface may change the physico-chemical nature of the substrate as discussed above (Fig. 3F).

In order to eliminate these inhibition effects from our analysis, we focus on the initial rates of the three experiments in the following analysis. We define the initial rate ($v_{init} = \Delta A_o/\Delta t_o$) as the change in internal area per time of a given hole between the two first scans (e.g. Fig. 1A and B). The number of individual structural defects was 22 in the experiment with $c_{HLL} = 2.5$ nM, 6 in the experiment with $c_{HLL} = 15$ nM and 6 in the experiment with $c_{HLL} = 45$ nM. Not all the structural defects were analysed as, e.g. structural defects, expanding beyond the AFM scan area could not be analysed. The initial rate of change in desorbed area of each structural defect has been deduced from the six images shown in Fig. 4. As stated previously, the rate of hydrolysis is found to be proportional to the perimeter length of the initial structural defects. Consequently, we

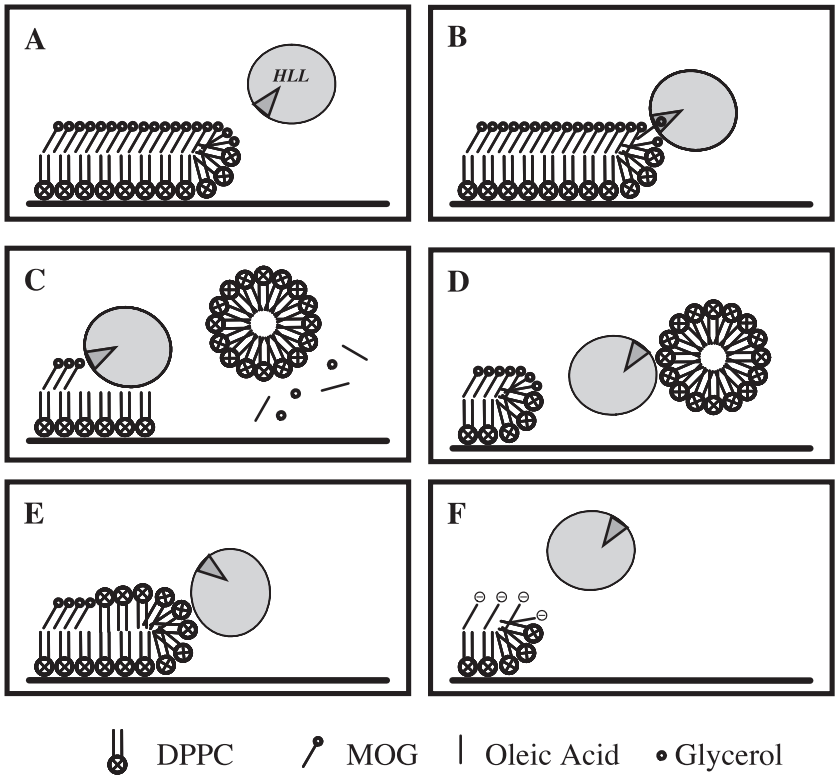

Fig. 3. Schematic illustration of the kinetic steps involved in the lipid bilayer desorption observed by AFM. (A) The enzyme adsorbs to the lipid film. (B) The enzyme is activated at the edge of structural defects. (C) Hydrolysis occurs in the hypothesized rate-limiting step, and spontaneously desorbed DPPC molecules form aggregates. Incomplete hydrolysis is likely to be caused by one or more of the following events: (D) Binding of HLL to DPPC aggregates either to soluble aggregates. (E) Binding to aggregates formed at the solid surface. (F) Changes in the physico-chemical properties of the interface due to fatty acid hydrolysis products remaining in the lipid film.

normalise the initial rate with respect to the initial perimeter. This will be referred to as the normalised initial rate in units of micrometers/minute. Due to the temporal resolution of the AFM, which is in the order of one measurement per 3 min, it is apparent that this method will give a lower estimate for the normalised initial rates, since inhibitory effects are likely to set in during the first scan. In Fig. 5A, the individual initial rates have been plotted versus the initial perimeter length of each hole to test Eq. (1). The fair linear correlation corroborates the assumption that the rate is proportional to the perimeter length for all values of P. The values for the 2.5 nM experiment, which are more scattered, are re-plotted on a more appropriate scale in Fig. 5B. The average normalised initial rates (v_{init}/P_o = slopes) for each series are plotted versus enzyme concentration in Fig. 6. The values in Fig. 6 show a strong linear correlation ($R^2 = 0.998$) in the bulk enzyme concentration range in question. Together, the data presented in Figs. 5 and 6 prove the validity of Eq. (1), and this in turn implies that the edges of the structural defects are not saturated with enzyme. In the case of saturation, the initial rate would be independent of the bulk enzyme concentration. The value for the 2.5 nM series is slightly below the fitted line. We believe that part of this is caused by non-specific binding of enzyme molecules (i) onto the sides of the container in which the solution was prepared, (ii) the syringe used to inject the enzyme into the liquid cell (iii) and the liquid cell.

There are several reasons for putting special emphasis on the 2.5 nM series. The series has many small initial defects present before enzyme injection (22 of these are analysed) and they present the unique opportunity of having many "separate experiments" under exactly the same conditions. Secondly, this is the only series where holes are observed to emerge from sites of no visible initial structural defect in the bilayer. We believe that most of the new holes start from structural defects that are too small to be imaged with AFM resolution. This is corroborated by the fact that some of the new holes start where dim shades are visible, which is likely to be holes that are too small to be penetrated by the AFM tip (AFM tip radius 5–30 nm). Some new holes emerge at sites which seem defect-free, but the relaxation of the lipid substrate discussed above makes the bilayer less dense and apparently facilitates enzyme access. The third reason for giving the 2.5 nM series special emphasis is that we see a very large spread in the measured initial rates (Fig. 5B) compared to the other experiments using higher enzyme concentration. The large spread can most likely be attributed to a stochastic distribution of single enzymes in the various structural defects due to the very low bulk concentration of

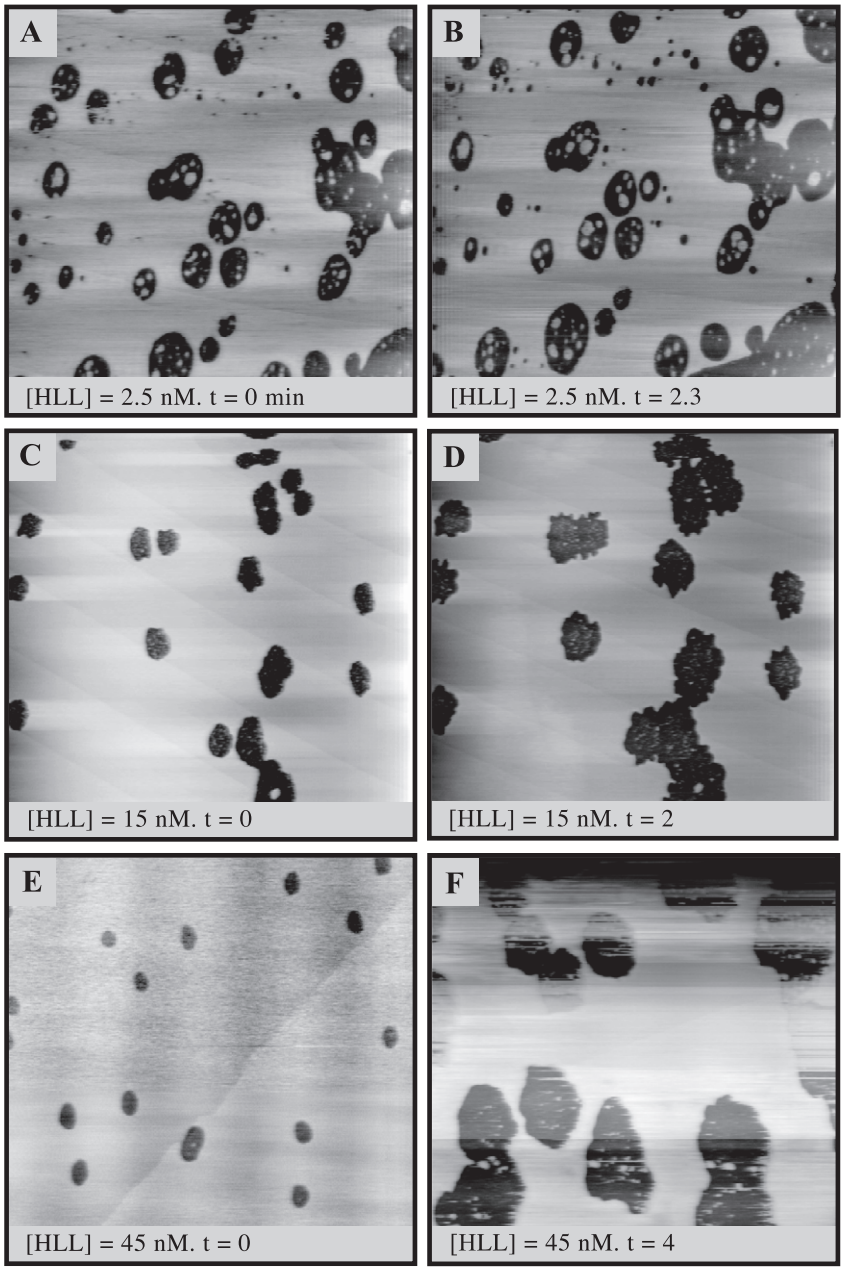

Fig. 4. The six images used to deduce the initial rate of hydrolysis. (A) The last image prior to injection and (B) the first image after injection of a 2.5 nM enzyme solution. (C,D) Two similar images injecting 15 nM enzyme solution. (E,F) Two similar images injecting 45 nM enzyme solution.

enzyme. A nominal enzyme concentration of 2.5 nM corresponds to 7.5×10^3 enzyme molecules in the scanning area volume with an average distance between each enzyme, $d_{3D}=(1/c_{HLL}\cdot N_A)^{1/3}$, in solution around 0.9 μm.

With all this in mind, it seems likely that the new holes that emerge in the bilayer are the result of single enzyme action. The average initial rates of these emerging holes are $\sim 1 \times 10^{-2}$ μm^2/min. Given that the mean molecular area of MOG at 25 mN/m is 40 Å^2 ($\approx 2.5 \times 10^6$ MOG molecules/μm^2), the specific activity of HLL-MOG hydrolysis is $\sim 2.5 \times 10^4$ lipid molecules/minute per enzyme molecule. Using this estimate, we can calculate the percentage of active enzymes in all the experiments. With a 2.5 nM enzyme concentration, we find a total degradation of 0.7 μm^2 of MOG in the first 2.3 min. Using an initial rate of 1×10^{-2} μm^2/min per enzyme, we estimate a total of 30 active enzymes in the scan area. If the injected amount of enzyme was 2.5 nM ($\sim 7.5 \times 10^3$ enzymes in the scanning volume) only 0.04% of the enzymes are active. The ''occupancy'' of active enzymes at the edge of structural defects can also be estimated; in the 2.5 nM experiment, the total edge length of structural defects in the scan area was 45 μm. If enzymes are sitting at the edge in a shoulder-to-shoulder fashion, each enzyme occupies approximately 5 nm of edge

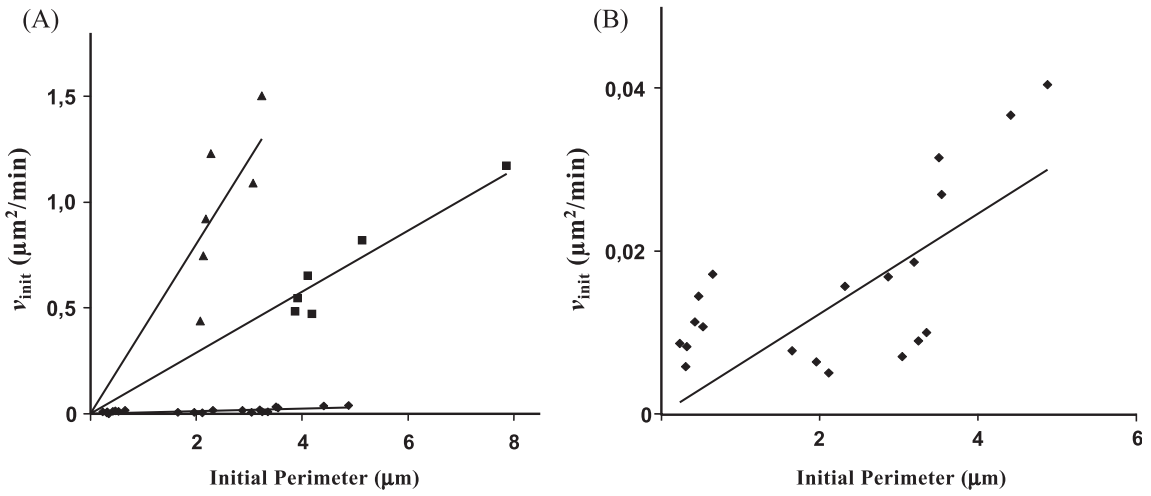

Fig. 5. (A) The change in desorbed area of the individual structural defects depicted in Fig. 4 plotted versus the initial perimeter length; 2.5 nM (♦), 15 nM (■) and 45 nM (▲). In general, the initial rate of the single structural defects is proportional to its initial perimeter length. (B) Blow-up of the data points from the 2.5 nM experiment.

[4]. This gives a total number of potential activation sites equal to the edge length/diameter of HLL (45 μm/5 nm) ~ 9×10^3. Of these, 30 are used yielding a 0.3% occupancy. These numbers for all three experiments are summarised in Table 1.

For comparison, Verger et al. have measured the specific activity of MOG hydrolysis by HLL (Table 2) using the zero-order trough technique (Verger, R. personal communication) [18]. The measured rates are in surprisingly good agreement with the measured AFM values, considering that there are some fundamental differences between the two experiments: (i) Verger et al. assume that 1% of the enzymes are active at the lipid–water interface, (ii) the zero-order trough experiments are carried out in Tris buffer close to HLL's pH optimum [17], (iii) β-cyclodextrin is added to the subphase to help remove products from the interface by binding them inside the water-soluble β-cyclodextrin molecules (in fact no hydrolysis is observed without β-cyclodextrin in the subphase), (iv) the substrate is under constant pressure keeping it defect-free, and (v) hydrolysis of MOG in the zero-order trough creates unfavourable air–water interface. Conversely, in the AFM experiment, it is assumed that most new holes in the lipid bilayer are caused by a single active enzyme in each of these holes. Also, the experiment is carried out in Milli-Q water below the pH activity optimum of HLL because Tris-buffer had been reported to induce the ripple phase in phospholipid bilayers [33], and β-cyclodextrin was dismissed because preliminary AFM experiments showed that the β-cyclodextrin solution in the AFM liquid cell induced holes in the DPPC/MOG bilayer. This latter effect is also observed and compensated for in the zero-order trough experiment, where both substrate molecules (MOG) and product molecules (oleic acid) are removed from the interface by β-cyclodextrin [18], and finally hydrolysis of MOG and desorption of

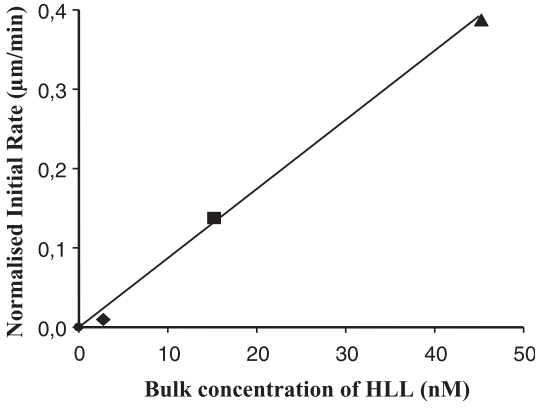

Fig. 6. The average initial rates for the three experiments (equal to the slopes of the lines in Fig. 5A) and the control experiment (enzyme concentration = 0, initial rate = 0) versus the concentration of enzyme injected.

Table 1
Summary of the three experiments

Concentration (nM)[a]	Number of active enzymes[b]	Total initial perimeter length (μm)[c]	Maximum number of accessible substrate sites[d]	Occupancy of perimeter (%)[e]
2.5	30	45	9.0×10^3	0.3
15	4.1×10^2	29	5.8×10^3	7
45	5.9×10^2	15	3.0×10^3	20

[a] Bulk concentration of enzyme solution injected into the liquid cell.
[b] Number of active enzymes in the scan area during the first scan (e.g. in the 2.5 nM experiment: $\Delta A_o/\Delta t_o \times$ initial rate of hydrolysis per enzyme molecule at the surface = 0.7 μm²/2.3 min × 0.01 μm²/min × enzyme molecule).
[c] The total measured perimeter length in the scan area.
[d] Maximum number of potential activation sites along the perimeter (= total perimeter length/diameter of an HLL enzyme molecule = 45 μm/5 nm = 9×10^3).
[e] Percentage of potential activation sites which is occupied by enzyme molecules (= $30/9 \times 10^3 \times 100\% = 0.3\%$).

Table 2
Comparison of experimental techniques

Experimental technique	Conditions	Initial rate of MOG hydrolysis (MOG/(min × $N_{HLL,active}$))
AFM	Milli-Q water	
	pH ~ 6.5	
	$c_{HLL,Bulk}$ = 2.5 nM	2.5×10^4
Zero-order trough	Tris buffer	
	pH ~ 8.0	
	$c_{HLL,Bulk}$ = 0.16 nM	
	$c_{\beta\text{-CD}}$ = 0.8 mg/ml	5.8×10^4

The experimental conditions and the initial rates of hydrolysis measured in the presented AFM experiment and calculated from the zero-order trough experiment reported in Ref. [18] (see text).

DPPC in the AFM liquid cell creates mica–water interface, which is energetically comparable to the initial lipid–water interface.

The obtained estimated specific activities are summarised in Table 2 showing that the zero-order trough value is in the order of 6×10^4 MOG *molecules/minute·enzyme molecule* and the AFM value is in the order of 2.5×10^4 MOG *molecules/minute·enzyme molecule*. The zero-order trough value is calculated from Fig. 5 in Ref. [18] by subtracting the slope of "decrease of surface area per minute" with only β-CD in the subphase and the slope of "decrease of surface area per minute" with both β-CD and HLL in the subphase of the zero-order trough, i.e. the increased rate of "decrease of surface area" after enzyme injection and assuming 1% of the bulk concentration of enzyme is active at the lipid–water interface.

Combining the observed phenomena of the AFM and zero-order trough experiments, it seems possible that the hydrolysis in the zero-order trough is directly related to holes in the monolayer that are induced by the β-cyclodextrin since we observe that intact lipid areas are resistant to enzyme attack, and that β-cyclodextrin induce holes in the bilayer. Although these holes are compensated for in the zero-order trough by compression of the barriers, the enzyme should have ample time to activate and start hydrolysis in these β-cyclodextrin-induced holes. It has earlier been reported [34] that the rate of desorption of the hydrolysis product (oleic acid) from the lipid–water interface becomes constant and independent of the β-cyclodextrin concentration above 0.5 mM β-cyclodextrin. However, if β-cyclodextrin induces holes in which the enzyme is activated, then the concentration of β-cyclodextrin could play a significant role.

From the AFM experiment, we estimate that approximately 0.05% of the enzymes in the bulk are active at the perimeter of the structural defects in the scan area. This is 20 times less than Verger et al.'s estimate of 1%. This indicates that if the estimated values from AFM and the zero-order trough experiments are both correct, then it is likely that there is 20 times less enzyme activating perimeter in the lipid monolayer in the zero-order trough than in the bilayer in the AFM.

4. Conclusions

Using the LB-technique, we prepared a lipid/phospholipid (MOG/DPPC) bilayer substrate with the lipid layer exposed to the aqueous phase. The substrate had a well-defined structure, and proved very suitable for both qualitative and quantitative analysis of interfacial lipolytic action. The substrate degradation by HLL was imaged in Milli-Q water using liquid cell AFM. The obtained images gave information of the preferred sites of enzymatic action. In two of three experimental series (using bulk enzyme concentrations of 15 and 45 nM), only initial structural defects were attacked by enzyme, confirming earlier experimental findings that HLL is activated by substrates with high curvature [14]. In the third experimental series using a HLL concentration of 2.5 nM, not only existing structural defects were attacked. Many new holes in the MOG layer were observed to emerge randomly in various areas during the first 30 min.

For all three concentrations of enzyme, we found that the rate of hydrolysis is proportional to the perimeter length of the initial structural defects in the bilayer and to the bulk enzyme concentration. This observation shows that the edge of the structural defects were not saturated with enzyme for all used concentrations of enzyme.

Finally, calculations based on an assumption that new holes which emerge from initially planer sites on the bilayer in the 2.5 nM series are a result of single enzyme action give an initial rate of hydrolysis $\sim 2.5.10^4$ MOG *molecules/minute* per enzyme molecule, which agrees well with estimates based on zero-order trough experiments.

The findings herein are consistent with earlier results regarding preferred sites of activation of PLA_2, which have been found to discriminate between structural and compositional defects [7,8].

Acknowledgements

We thank Shamkant Anant Patkar, Novozymes A/S, for purifying all enzyme samples. Financial support from the European Community through the project: Lipid structure and lipases, BIO4 CT 972365, and the Danish Research Council is gratefully acknowledged. We thank Dr. Robert Verger for fruitful discussions.

References

[1] G. Binnig, C.F. Quate, C. Gerber, Atomic force microscope, Physical Review Letters 56 (1986) 930–933.
[2] Z. Reich, R. Kapon, R. Nevo, Y. Pilpel, S. Zmora, Y. Scolnik, Scanning force microscopy in the applied biological sciences, Biotechnology Advances 19 (2001) 451–485.
[3] C.B. Prater, H.J. Butt, P.K. Hansma, Atomic force microscopy, Nature 345 (1990) 839–840.
[4] K. Balashev, T.R. Jensen, K. Kjaer, T. Bjørnholm, Novel methods for

studying lipids and lipases and their mutual interaction at interfaces: Part I. Atomic force microscopy, Biochimie 83 (2001) 387–397.
[5] M. Radmacher, M. Fritz, H.G. Hansma, P.K. Hansma, Direct observation of enzyme-activity with the atomic-force microscope, Science 265 (1994) 1577–1579.
[6] M. Grandbois, H. Clausen-Schaumann, H. Gaub, Atomic force microscope imaging of phospholipid bilayer degradation by phospholipase A(2), Biophysical Journal 74 (1998) 2398–2404.
[7] L.K. Nielsen, J. Risbo, T.H. Callisen, T. Bjørnholm, Lag-burst kinetics in phospholipase A(2) hydrolysis of DPPC bilayers visualized by atomic force microscopy, Biochimica et Biophysica Acta 1420 (1999) 266–271.
[8] L.K. Nielsen, K. Balashev, T.H. Callisen, T. Bjørnholm, Influence of product phase separation on phospholipase A2 hydrolysis of supported phospholipid bilayers studied by force microscopy, Biophysical Journal 83 (2002) 2617–2624.
[9] D.M. Lawson, A.M. Brzozowski, G.G. Dodson, R.E. Hubbard, B. Huge-Jensen, E. Boel, Z.S. Derewenda, in: P. Woolley, S.B. Petersen (Eds.), Lipases; Their Structure, Biochemistry and Application, Cambridge Univ. Press, Cambridge, 1994, pp. 77–95.
[10] K. Thirstrup, R. Verger, F. Carriere, Evidence for a pancreatic lipase subfamily with new kinetic-properties, Biochemistry 33 (1994) 2748–2756.
[11] I. Panaiotov, R. Verger, Physical chemistry of biological interfaces, in: A.W.N.W. Bazkin (Ed.), Marcel Dekker, New York, 2000, pp. 359–400.
[12] A. Svendsen, Lipase protein engineering, Biochimica et Biophysica Acta. Protein Structure and Molecular Enzymology 1543 (2000) 223–238.
[13] O.G. Berg, Y. Cajal, G.L. Butterfoss, R.L. Grey, M.A. Alsina, B.Z. Yu, M.K. Jain, Interfacial activation of triglyceride lipase from *Thermomyces* (*Humicola*) *lanuginosa*: kinetic parameters and a basis for control of the lid, Biochemistry 37 (1998) 6615–6627.
[14] Y. Cajal, A. Svendsen, J. De Bolos, S.A. Patkar, M.A. Alsina, Effect of the lipid interface on the catalytic activity and spectroscopic properties of a fungal lipase, Biochimie 82 (2000) 1053–1061.
[15] M. Norin, O. Olsen, A. Svendsen, O. Edholm, K. Hult, Theoretical studies of *Rhizomucor miehei* lipase activation, Protein Engineering 6 (1993) 855–863.
[16] G.H. Peters, S. Toxvaerd, O.H. Olsen, A. Svendsen, Computational studies of the activation of lipases and the effect of a hydrophobic environment, Protein Engineering 10 (1997) 137–147.
[17] R.D. Schmid, R. Verger, Lipases: interfacial enzymes with attractive applications, Angewandte Chemie. International Edition 37 (1998) 1609–1633.
[18] M. Ivanova, A. Svendsen, R. Verger, I. Panaiotov, Action of *Humicola lanuginosa* lipase on long-chain lipid substrates: 1. Hydrolysis of monoolein monolayers, Colloids and Surfaces. B, Biointerfaces 26 (2002) 301–314.
[19] R. Verger, G.H.D. Haas, Enzyme reactions in a membrane model: 1. New technique to study enzyme reactions in monolayers, Chemistry and Physics of Lipids 10 (1973) 127–136.
[20] S. Ransac, H. Moreau, C. Riviere, R. Verger, Monolayer techniques for studying phospholipase kinetics, Methods in Enzymology 197 (1991) 49–65.
[21] R. Verger, G.H. Dehaas, Interfacial enzyme-kinetics of lipolysis, Annual Review of Biophysics and Bioengineering 5 (1976) 77–117.
[22] H.L. Brockman, F.J. Kezdy, J.H. Law, Isobaric titration of reacting monolayers—kinetics of hydrolysis of glycerides by pancreatic lipase-B, Journal of Lipid Research 16 (1975) 67–74.
[23] W.E. Momsen, H.L. Brockman, Recovery of monomolecular films in studies of lipolysis, Lipases, Pt B 286 (1997) 292–305.
[24] M. Ivanova, R. Verger, I. Panaiotov, Mechanisms underlying the desorption of long-chain lipolytic products by cyclodextrins: application to lipase kinetics in monolayer, Colloids and Surfaces. B, Biointerfaces 10 (1997) 1–12.
[25] T.R. Jensen, K. Kjaer, in: D. Mõbius, R. Miller (Eds.), Novel Methods to Study Interfacial Layers, Elsevier, New York, 2001, pp. 205–254.
[26] J.M.R. Patino, C.C. Sanchez, M.R.R. Nino, Morphological and structural characteristics of monoglyceride monolayers at the air–water interface observed by Brewster angle microscopy, Langmuir 15 (1999) 2484–2492.
[27] T.R. Jensen, K. Kjaer, P.B. Howes, A. Svendsen, K. Balashev, N. Reitzel, T. Bjørnholm, Model systems for biological membranes investigated by grazing—incidence X-ray diffraction and specular reflectivity, in: G. Kokotos, V. Constantinou-Kokotou (Eds.), Proceedings of Lipids and Lipases, Crete Univ. Press, Rethymnon, Santorini, Greece, 1999, p. 27.
[28] F. Beisson, A. Tiss, C. Riviere, R. Verger, Methods for lipase detection and assay: a critical review, European Journal of Lipid Science and Technology 102 (2000) 133–153.
[29] J.N. Israelachvili, Intermolecular and Surface Forces, 2nd ed., Academic Press, London, 1992.
[30] Y. Cajal, A. Svendsen, V. Girona, S.A. Patkar, M.A. Alsina, Interfacial control of lid opening in *Thermomyces lanuginosa* lipase, Biochemistry 39 (2000) 413–423.
[31] G.H. Peters, U. Dahmen-Levison, K. de Meijere, G. Brezesinski, S. Toxvaerd, H. Mohwald, A. Svendsen, P.K.J. Kinnunen, Influence of surface properties of mixed monolayers on lipolytic hydrolysis, Langmuir 16 (2000) 2779–2788.
[32] A.M. Brzozowski, H. Savage, C.S. Verma, J.P. Turkenburg, D.M. Lawson, A. Svendsen, S. Patkar, Structural origins of the interfacial activation in *Thermomyces* (*Humicola*) *lanuginosa* lipase, Biochemistry 39 (2000) 15071–15082.
[33] J.X. Mou, J. Yang, Z.F. Shao, Tris(Hydroxymethyl)aminomethane (C4H11No3) induced a ripple phase in supported unilamellar phospholipid-bilayers, Biochemistry 33 (1994) 4439–4443.
[34] M.G. Ivanova, T. Ivanova, R. Verger, I. Panaiotov, Hydrolysis of monomolecular films of long chain phosphatidylcholine by phospholipase A(2) in the presence of beta-cyclodextrin, Colloids and Surfaces. B, Biointerfaces 6 (1996) 9–17.